International Journal of Heat and Mass Transfer 183 (2022) 122012

Contents lists available at ScienceDirect

International Journal of Heat and Mass Transfer

journal homepage: www.elsevier.com/locate/hmt

# Predicting vapour transport from semi-volatile organic compounds concealed within permeable packaging

Timothy Foat[a,b,*], Joseph Drodge[a], Alexandra Charleson[a], Barry Whatmore[a], Sophie Pownall[a], Peter Glover[a], James Nally[a], Simon Parker[a], Catherine Khan[a], Andrew Marr[a]

[a] Dstl, Porton Down, Salisbury, Wiltshire SP4 0JQ, UK
[b] Faculty of Engineering and Physical Sciences, University of Southampton, Hampshire SO17 1BJ, UK

ARTICLE INFO

*Article history:*
Received 3 May 2021
Revised 24 August 2021
Accepted 23 September 2021

*Keywords:*
SVOC
Sorption
Permeation
Computational fluid dynamics
Explosives
Detection

ABSTRACT

The vapour concentration present in enclosed spaces containing concealed semi-volatile organic compounds (SVOCs), such as explosives, is difficult to measure experimentally. Therefore, mathematical models play a key role in understanding the transport of these materials. Vapour transport has previously been modelled in a range of environments, from small emission cells to whole rooms, using both analytical and numerical approaches. These models typically include either a well-mixed air volume or a simple sorption model. This work has been extended by including a multi-layer vapour sorption/permeation model within a computational fluid dynamics (CFD) framework. This allows for vapour source terms from items concealed within permeable packaging to be considered. The CFD based permeation model includes sorption/desorption, using a linear isotherm at inner and outer surfaces and a blended wall function to account for the effects of near-wall turbulence. The model has been validated for the explosive SVOC, ethylene glycol dinitrate (EGDN). The model has been used to show how vapour concentrations around a cardboard box containing a SVOC vary when some of the key input parameters are changed. Changing the vapour source from EGDN to the much lower vapour pressure trinitrotoluene (TNT), had a significant effect, as expected, and this was most pronounced early on due to the difference in permeation lag times for the two materials. Conversely, changing the type of cardboard had only a small effect on the concentrations. This type of modelling approach can now be used to study a wide range of SVOC transport problems which would not previously have been possible.



## 1. Introduction

The transport of vapour from semi-volatile organic compounds (SVOCs) (i.e. an organic compound with a vapour pressure between $10^{-9}$ Pa and 10 Pa [1]) is of interest in a number of different fields, including health [1,2] and the detection of explosives [3,4]. Many mathematical models have been produced to predict the transport of vapour from both SVOCs and volatile organic compounds (VOCs). Most models employ a well-mixed approach with no variation in concentration across the air space [5–9]. Others use computational fluid dynamics (CFD) to provide the spatial resolution. Spatial resolution can be critical as vapour concentrations may reduce by orders of magnitude within a very short distance from the source [4], therefore, average concentrations are not representative of the entire space. This information is of interest in explosives detection applications when the detector may be sampling from either high or low concentration regions. Understanding how explosives vapour concentrations vary within a space can help to improve search and screening methodologies. CFD has been used to model systems ranging in size from emission cells with volumes of a few litres or less [10,11] and a dog's nose [12], to room scale [13–17]. Of those using CFD, sorption has been considered using a range of different approaches. Mao et al. [10] and Clausen et al. [11] used a linear adsorption isotherm and Murakami et al. [14] applied three different adsorption isotherm models. Lawson

* Corresponding author at: Dstl, Porton Down, Salisbury, Wiltshire SP4 0JQ, UK.
*E-mail addresses:* tgfoat@dstl.gov.uk (T. Foat), jdrodge1@dstl.gov.uk (J. Drodge), acharleson@dstl.gov.uk (A. Charleson), bwhatmore@dstl.gov.uk (B. Whatmore), spownall@dstl.gov.uk (S. Pownall), pbglover@dstl.gov.uk (P. Glover), jnally@dstl.gov.uk (J. Nally), stparker@dstl.gov.uk (S. Parker), cckhan@dstl.gov.uk (C. Khan), ajmarr@dstl.gov.uk (A. Marr).

https://doi.org/10.1016/j.ijheatmasstransfer.2021.122012

**Nomenclature**

| | |
|---|---|
| $a$ | mass transfer coefficient [m s$^{-1}$] |
| $A$ | area [m$^2$] |
| $C$ | species concentration [kg m$^{-3}$] |
| $C_0$ | volatility of substance [kg m$^{-3}$] |
| $C^*$ | species concentration at the wall [kg m$^{-3}$] |
| $C_i$ | species concentration in the solid, in layer $i$ [kg m$^{-3}$] |
| $C_{in}$ | inlet species concentration [kg m$^{-3}$] |
| $C_{out}$ | outlet species concentration [kg m$^{-3}$] |
| $C_p$ | species concentration in the near-wall cell [kg m$^{-3}$] |
| $C_{surf}$ | species concentration on the surface [kg m$^{-2}$] |
| $C_\mu$ | constant [dimensionless] |
| $d_{layer}$ | thickness of the individual permeation layers [m] |
| $D_m$ | molecular diffusion coefficient [m$^2$ s$^{-1}$] |
| $D_{solid}$ | solid phase diffusion coefficient [m$^2$ s$^{-1}$] |
| $d_{total}$ | total thickness of the permeable solid [m] |
| $E$ | constant[dimensionless] |
| $F$ | species flux [kg m$^{-2}$ s$^{-1}$] |
| $K_{ab}$ | solubility or partition coefficient [dimensionless] |
| $K_{ad}$ | partition coefficient [m] |
| $k_p$ | turbulent kinetic energy in the near-wall cell [m$^2$ s$^{-2}$] |
| $k_{vkc}$ | von Karman constant [dimensionless] |
| $n_{layer}$ | number of permeation layers |
| $P_c$ | constant[dimensionless] |
| $Sc$ | Schmidt number [dimensionless] |
| $Sc_t$ | turbulent Schmidt number[dimensionless] |
| $t$ | time [s] |
| $t_{lag}$ | time lag (permeation time constant) [s] |
| $T$ | temperature [°C] |
| $U$ | mean velocity [m s$^{-1}$] |
| $y^*$ | non-dimensional near-wall distance based on turbulent kinetic energy |
| $y^+$ | non-dimensional near-wall distance based on friction velocity |
| $y_1$ | near-wall distance for the near-wall cell [m] |
| $Y^+_{BWF}$ | normalised species mass fraction [dimensionless] |
| $Y^+_{lam}$ | laminar component of $Y^+_{BWF}$ [dimensionless] |
| $Y^+_{turb}$ | turbulent component of $Y^+_{BWF}$ [dimensionless] |
| $Y_w$ | species mass fraction at the wall [kg kg$^{-1}$] |
| $Y_p$ | species mass fraction in the near-wall cell [kg kg$^{-1}$] |
| *Greek symbols* | |
| $\Gamma$ | blending function[dimensionless] |
| $\Delta t$ | time step size [s] |
| $\mu$ | dynamic viscosity [kg m$^{-1}$ s$^{-1}$] |
| $\rho$ | fluid density [kg m$^{-3}$] |

et al. [12] modelled one-way sorption with diffusion to a surface sink.

When the air flow in the space is modelled in detail, studies have considered both laminar [10,11] and turbulent flows [14]. However, even in the work of Murakami et al. [14], where the air flow in the room was turbulent, the mesh was refined in the near-wall region to place the first cell in the viscous sub-layer. This meant that a simple Fick's law model could be used represent vapour transport from the wall-adjacent cell to and from the wall.

In this study a new CFD based multi-layer vapour sorption/permeation model has been tested and applied. It used a linear isotherm to represent absorption, diffusion through internal layers and then the same linear isotherm for desorption on the other side of the solid if required. The input data for the sorption/permeation model, solid phase diffusion coefficient, $D_{solid}$ [m$^2$ s$^{-1}$] and a dimensionless solubility or partition coefficient, $K_{ab}$, can be measured easily using a standard permeation cell set-up. An absorption model based on partitioning followed by diffusion is also more physically representative than the sink-diffusion model of Jørgensen et al. [18] or the three-layer model of Singer et al. [6]. Zhang et al. [19] also commented that it might not be possible to measure the input parameters for the Jørgensen et al. model directly. The Singer et al. [6] and Jørgensen et al. [18] models do have a possible advantage over the model proposed here in that they do not require the depth of the permeable solid to be specified.

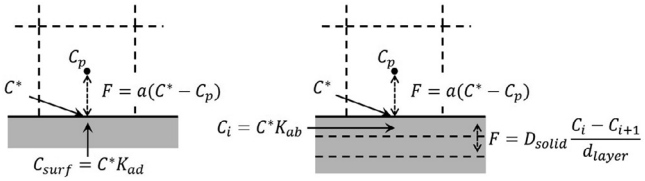


**Fig. 1.** Diagram showing the implementation of the adsorption (left) and absorption/permeation models (right).

The model uses a blended wall function to account for the effects of near-wall turbulence so can be applied whether the near-wall cell is in the linear region or the log-law region.

The model has been validated using test cases of increasing complexity, using the SVOC explosive ethylene glycol dinitrate (EGDN) as the vapour sources.

This new modelling framework can be used to study SVOC and VOC vapour transport in a range of environments.

## 2. Mathematical model

### 2.1. Sorption/permeation model

The sorption/permeation models were implemented as illustrated in Fig. 1, based on the framework originally developed by Nally et al. [20]. The vapour is transported from the near-wall cell, where the concentration is $C_p$ [kg m$^{-3}$], to a point close to the wall where the concentration, $C^*$ [kg m$^{-3}$], is in equilibrium with the surface concentration, $C_{surf}$ [kg m$^{-2}$] or solid phase concentration $C_i$ [kg m$^{-3}$]. The flux between $C_p$ and $C^*$ is governed by the mass transfer coefficient, $a$ [m s$^{-1}$] and the concentration gradient. $C^*$ is related to $C_{surf}$ or $C_i$ by a partition coefficient, $K_{ad}$ [m] or $K_{ab}$ [dimensionless]. For the absorption or permeation model, there is a flux between layers in the solid which is governed by the solid phase diffusion coefficient, $D_{solid}$, and the concentration in adjacent layers. For permeation, the vapour can return back to the gas phase from the outer side of the permeable material using the same processes as applied when it entered the solid phase, but in reverse.

When the flow is turbulent, the mass transfer coefficient is calculated using a blended wall function model [21]. In this model, the normalised species mass fraction, $Y^+_{BWF}$ [dimensionless], is given by the follow equation,

$$Y^+_{BWF} \equiv \frac{(Y_w - Y_p)\rho C_\mu^{1/4} k_p^{1/2}}{F} = \exp(\Gamma) Y^+_{lam} + \exp(1/\Gamma) Y^+_{turb}, \qquad (1)$$

where $Y_w$ [kg kg$^{-1}$] is the species mass fraction at the wall, $Y_p$ [kg kg$^{-1}$] is the mass fraction at the centroid of the first cell, $\rho$ [kg m$^{-3}$] is the fluid density, $C_\mu$ is a dimensionless constant (0.09), $k_p$ [m$^2$ s$^{-2}$] is the turbulent kinetic energy (TKE) in the near-wall cell and $F$ [kg m$^{-2}$ s$^{-1}$] is the flux. $Y_w$ and $Y_p$ can be converted to concentrations $C^*$ and $C_p$ by multiplying by $\rho$. The blending func-

tion, Γ [dimensionless] is given by the following equation,

$$\Gamma = -\frac{0.01(Sc\,y^*)^4}{1+5Sc^3y^*}, \tag{2}$$

where $Sc$ is the non-dimensional Schmidt number. The non-dimensional near-wall cell height, $y^*$, is given by the following equation,

$$y^* \equiv \frac{\rho C_\mu^{1/4} k_p^{1/2} y_1}{\mu}, \tag{3}$$

where $y_1$ [m] is the distance from the wall to the centroid of the near-wall cell and $\mu$ [kg m$^{-1}$ s$^{-1}$] is the dynamic viscosity.

The laminar component of the normalised species mass fraction, $Y^+_{lam}$, is given in Eq. (4) and the turbulent component, $Y^+_{turb}$, in Eq. (5).

$$Y^+_{lam} = Sc\,y^* \tag{4}$$

$$Y^+_{turb} = Sc_t\left[\frac{1}{k_{vkc}}\ln(E\,y^*) + P_c\right], \tag{5}$$

where $Sc_t$ is the non-dimensional turbulent Schmidt number, $E$ is a dimensionless empirical constant (9.793), $k_{vkc}$ is the von Karman constant (0.42 has been used here). $P_c$ is an dimensionless empirical constant, which is given by Eq. (6) [22].

$$P_c = 9.24\left[\left(\frac{Sc}{Sc_t}\right)^{3/4} - 1\right][1 + 0.28\exp(-0.007Sc/Sc_t)] \tag{6}$$

The mass transfer coefficient between the near-wall cell and the wall, $a$, is given by Eq. (7).

$$a = \frac{F}{C^* - C_p} = \frac{F}{(Y_w - Y_p)\rho} \tag{7}$$

Eqs. (1) and (7) can then be rearranged to give

$$a = \frac{C_\mu^{1/4} k_p^{1/2}}{Y^+_{BWF}}, \tag{8}$$

If the flow is laminar or there is no air movement (i.e. molecular diffusion only), then $a$ can by calculated using the following equation,

$$a = \frac{D_m}{y_1}, \tag{9}$$

where $D_m$ [m$^2$ s$^{-1}$] is the molecular diffusion coefficient.

After the mass transfer coefficient $a$ is found, $C^*$ is calculated from the concentration on the surface or in the solid using a linear isotherm model. The flux to the surface, $F$ is then calculated as shown in Fig. 1 to give a new surface or solid concentration. If required, the concentrations in the permeation layers of the solid are then calculated using an implicit second-order finite difference method to solve Fick's second law of diffusion. $C^*$ is then recalculated from the new surface or solid concentration. This process is iterated until a converged solution is reached for the current time step. $C_p$ is then adjusted according to the flux by applying a source or sink term in the wall adjacent cell.

The sorption/permeation models were written as User Defined Functions (UDFs) in the ANSYS® Fluent® CFD software (hereon referred to as Fluent). The User Defined Memory (UDM) functionality in Fluent was used to store the vapour concentration (at the current and previous time steps) on the surface or in each permeation layer in the solid.

### 2.2. Air flow and vapour transport

The air flow and vapour transport was modelled using Fluent V15.0. A single model was also run in Fluent V18.0 and there was negligible difference between the results. Both laminar and turbulent flow models were run. For the turbulent flow models the $k-\omega$ shear-stress transport (SST) turbulence model [23] was used.

For all models, the flow was solved first as steady-state, the flow was then held constant and the vapour transport was solved transiently. The vapour was modelled as a passive scalar with $Sc_t = 0.7$.

A coupled solver was used for the pressure-velocity coupling. A second-order scheme was used for the pressure terms and a second-order upwind scheme for the convection terms in the momentum equation. The species and the turbulence convection terms were solved using a first-order upwind scheme and a first-order implicit scheme was used for the transient species transport. Previous work has shown that first-order schemes can give reasonable results for indoor air flows, therefore, this was used as a starting condition for the validation modelling.

Test models were re-run using second-order discretisation for the species convection terms and a second-order implicit scheme for the temporal discretisation. This had little effect on the concentration predictions, which was due to the high resolution in space and time applied in the model.

## 3. Model validation

The sorption/permeation model was validated using three test cases of increasing complexity. The first was laminar flow of vapour through a chamber with thick permeable walls. The second was the permeation of a vapour into, and laminar flow through, the same permeable chamber. The final case was permeation of vapour through a cardboard box into a room. This final set-up included permeation and adsorption with both laminar and turbulent regions.

### 3.1. Validation set-up

#### 3.1.1. Flow of vapour through a chamber with permeable walls

The first experiment consisted of a cylindrical polytetrafluoroethylene (PTFE) chamber (0.2 m long, 0.08 m inner diameter, 0.01 m wall thickness) into which EGDN vapour, at a concentration (averaged of measured concentrations), $C_{in} = 8.8\times10^{-7}$ kg m$^{-3}$, was supplied (see Fig. 2(a)). The EGDN vapour was generated using a temperature controlled KIN-TEK, C0395 vapour generator (KIN-TEK Analytical, Inc., Texas, USA) and mixed with dry nitrogen. The flow rate through the PTFE chamber (average of measured flow rates) was 0.1 L min$^{-1}$ at a temperature of 35 °C. The velocity through the narrow inlet tube (inner diameter $4.6\times10^{-3}$ m) was 0.1 m s$^{-1}$ and the average velocity across the full diameter of the chamber was $3.5\times10^{-4}$ m s$^{-1}$. This gave a Reynolds number of less than 2. The PTFE chamber was held in a temperature-controlled box (LABCOLD™ RPDF0012D, Labcold, Hampshire, UK).

The vapour concentration at the outlet of the chamber was monitored over 5 h by periodically taking 1 min gas samples, of approximately 0.1 L, using Tenax™ air sampling tubes. The sample tubes were analysed by thermal desorption gas chromatography mass spectrometry (Agilent 7890A GC, 5975C MSD, Agilent, California, USA). The experiment was repeated twice with triplicate measurements taken at each sample time.

In between experimental replicates, the surfaces of the chamber were cleaned with a combination of propan-2-ol (IPA) and acetone to remove EGDN residues. The chamber was then dried at a temperature of 50 °C for at least two hours before being cooled, reassembled and stabilised at experimental temperatures. During temperature stabilisation the chamber was flushed with dry nitrogen gas. Chamber outputs were measured prior to recommencing experimentation to ensure that there was no residual EGDN remaining within the chamber.

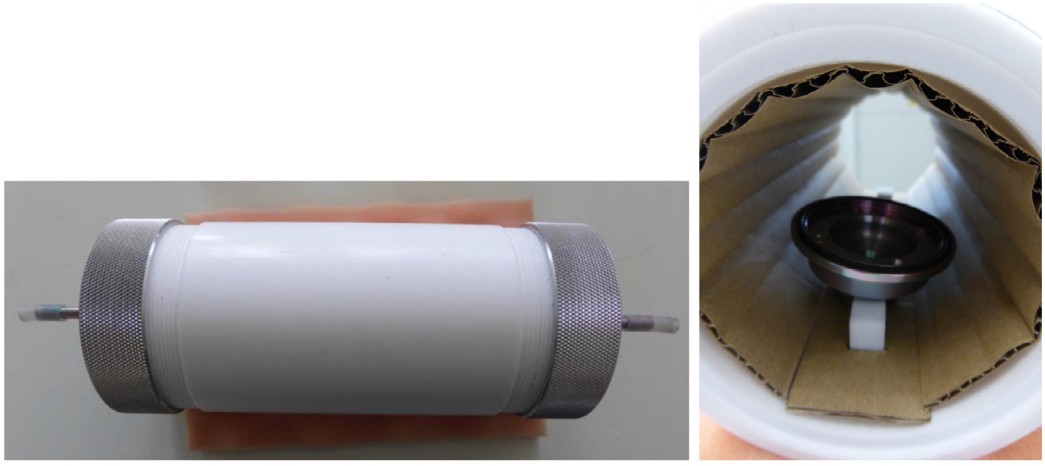


**Fig. 2.** The PTFE chamber. (a) the outside of the PTFE chamber as used in the first and second validation experiments. (b) the inside of the chamber with the cardboard lining and the PE sealed permeation accessory as used in the second validation experiments.

**Table 1**
Vapour parameters for EGDN permeation used in the model of the first validation experiment at 35 °C.

| | $D_m$/m$^2$ s$^{-1}$ | $D_{solid}$/m$^2$ s$^{-1}$ | $K_{ab}$ |
|---|---|---|---|
| EGDN | $9.3 \times 10^{-6}$ | | |
| PTFE | | $7.5 \times 10^{-14}$ | $1.2 \times 10^{3}$ |

The permeation properties for EGDN and PTFE at 35 °C were measured using a Micro-Chamber/Thermal Extractor™ (μ-CTE™) system with a permeation accessory (Markes International, Llantrisant, UK). The permeation accessory holds a thin layer of the material under investigation with the vapour source placed in a well below. The air flow over the top of the accessory is controlled by the Micro-Chamber and vapour samples are collected onto Tenax™air sampling tubes. $D_{solid}$ can then be calculated from the lag time, $t_{lag}$ [s], a time constant related to the point at which a constant permeation rate is achieved. The lag time is given by the following, $t_{lag} = d_{total}^2 \,/\, 6D_{solid}$, where $d_{total}$ [m] is the total thickness of the permeable solid. The partition coefficient (or solubility), $K_{ab}$, can then be calculated from the equilibrium permeation rate using Fick's first law. The permeation data produced is shown in Table 1. When applying permeation data generated using this method there is an assumption that $D_{solid}$ and $K_{ab}$ are not functions of the thickness of the permeable material.

The molecular diffusion coefficient for EGDN was calculated using a method based on atomic diffusion volumes [24] and this data is shown in Table 1.

The set-up for the CFD model was as follows. A 2-dimensional axi-symmetric, laminar CFD model of the PTFE chamber was produced. The laminar wall function option, Eq. (9), was specified in the UDF. The mesh consisted of unstructured tetrahedra, with a maximum cell edge length of 5 mm. The time step, $\Delta t$, for the vapour transport was set to 0.05 s for the first 2 s and was then increased to 0.1 s. With these settings it had been shown in a similar model that the concentration prediction showed little sensitivity to a reduction in the cell size or $\Delta t$. The inlet had a constant concentration boundary condition. The PTFE walls of the chamber were defined as permeable boundaries, with concentration fixed at zero on the outer wall. A diagram of the model is shown in Fig. 3.

The vapour permeation can be sensitive to the thickness of the individual permeation layers, $d_{layer}$. $d_{layer}$ was defined by specifying the total thickness of the solid, $d_{total}$, and the number of layers, $n_{layer}$ ($d_{layer} = d_{total}/n_{layer}$). The models were run with different values for $n_{layer}$ to find the point at which the models were no longer sensitive to $d_{layer}$. The results are most sensitive to $d_{layer}$ at the very early stage of the simulation. As the equilibrium flux is approached, the sensitivity decreases.

The results of this model converged once $d_{layer}$ for the walls of the PTFE chamber reached $1 \times 10^{-5}$ m. As the maximum number of UDMs in Fluent is 500, there is a limit to the number of permeation layers which can be defined. In this case $n_{layer}$ was set to 100 and therefore the total thickness, $d_{total}$, was 1 mm. The $d_{total}$ specified was much smaller than the actual wall thickness of the PTFE chamber walls (10 mm). However, $t_{lag}$ for even a 1 mm thick sheet of PTFE at 35 °C is 620 h, i.e. significantly longer than the duration of the experiment (5 h). In other words, during the experiment, the vapour will have been able to permeate only a small distance into the PTFE. Therefore, the outer region of the PTFE walls played little part in the permeation process. The results here were shown to be insensitive to an increase in $n_{layer}$ (for a fixed $d_{total}$). Therefore, a thick permeable material can be represented in the model by a thinner material if the duration of the simulation is short compared to the lag time.

### *3.1.2. Permeation of a vapour into and through a chamber with permeable walls*

The second experiment consisted of the same PTFE tube as used in the previous experiment, through which dry nitrogen at 30 °C was pumped at a nominal flow rate of 0.1 L min$^{-1}$. The tube was either lined with single thickness corrugated cardboard (see Fig. 2(b)) or was left unlined. The cardboard was $2.9 \times 10^{-3}$ m thick or $0.5 \times 10^{-3}$ m thick when the three layers of which it consisted were compressed together.

A source of EGDN vapour (10% w/w of EGDN on an inert material, Kieselguhr) was placed in a Markes permeation accessory which was sealed with a $130 \times 10^{-6}$ m thick film of polyethylene (PE). The permeation cell was made of Silcosteel®, an amorphous silicon coated steel, which was shown (data is not reported here) to adsorb a negligible amount of the vapour at 30 °C.

The EGDN was placed within the permeation accessory and was held at 30 °C for 1 h to allow the flux out of the permeation cell to equilibrate before being placed in the PFTE chamber.

The EGDN vapour concentration was measured at the outlet of the chamber (using the same method as for the previous experiment) periodically over a period of 4 h for the unlined chamber and for 24 h for the cardboard lined chamber. Three repeat experi-

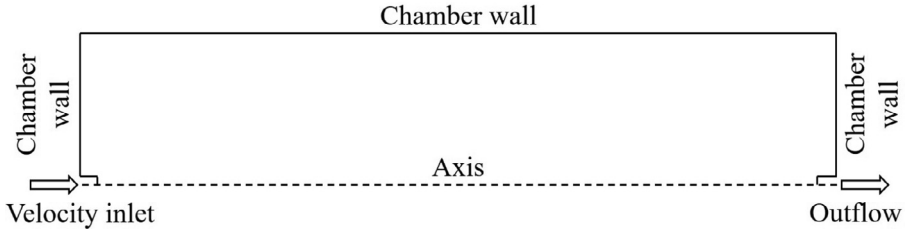


**Fig. 3.** Diagram showing the model geometry for the first validation experiment. Chamber dimension are given at the start of Section 3.1.1.

**Table 2**
Vapour parameters for EGDN permeation used in the model for the second validation experiment at 30 °C.

| | $C_0$/kg m$^{-3}$ | $D_m$/m$^2$ s$^{-1}$ | $D_{solid}$/m$^2$ s$^{-1}$ | $K_{ab}$ |
|---|---|---|---|---|
| EGDN | $9.7 \times 10^{-4}$ | $9.0 \times 10^{-6}$ | | |
| PTFE | | | $5.0 \times 10^{-14}$ | $1.4 \times 10^{3}$ |
| PE | | | $2.5 \times 10^{-12}$ | $1.9 \times 10^{3}$ |
| Corrugated card | | | $2.0 \times 10^{-11}$ | $1.7 \times 10^{3}$ |

ments were conducted with triplicate measurements taken at each sample time. Each sample was collected for 1 min.

The permeation properties for EGDN through PTFE, PE and cardboard and the molecular diffusion coefficient for EGDN were calculated or measured using the same method as described previously. The volatility was calculated using data from the review paper of Ewing et al. [3]. All these parameters are given in Table 2.

For this study, it was assumed that permeation of the low concentration EGDN vapour through cardboard could be approximated by a Fick's first law model.

The average flow rate for the unlined experiments was 0.094 L min$^{-1}$, for the cardboard lined experiments it was 0.079 L min$^{-1}$.

The set-up for the CFD model was as follows. A symmetric half of the chamber was represented using a laminar model. The laminar wall function option (Eq. (9)) was selected in the UDF along with the permeation model for PE, PTFE and cardboard.

The mesh used used mainly unstructured tetrahedrons and only a symmetric half of the geometry was modelled. 1mm hexahedral cells were applied to the inside of the permeation accessory. The maximum cell edge length in the chamber was 5 mm (as specified in the first validation experiment model). The time step size was kept at a constant 0.05 s for the unlined chamber and 0.03 s for the cardboard lined chamber. The slight reduction in $\Delta t$ for the cardboard lined chamber model compared to the unlined chamber model was due to an instability in the UDF when a larger $\Delta t$ was used. This was likely caused by the larger partition coefficient for cardboard compared to PTFE (see Table 2). It should be noted that all models were shown to be insensitive to a further reduction in $\Delta t$. The mesh around the permeation accessory was shown to be sufficiently well resolved to correctly predict the vapour flux through the PE film, i.e. a reduction in the size of the cells around the accessory did not affect the flux.

As with the model for the 1st validation experiment, the walls of the chamber were defined as permeable boundaries, with values of $D_{solid}$ and $K_{ab}$ specified. The concentration on the outer wall was fixed at zero and the inlet had a zero-concentration boundary condition. A diagram of the model is shown in Fig. 4.

To assess a simplified form of the model for the cardboard line chamber, the cardboard was included by applying the relevant permeation parameters to the chamber walls in place of the PTFE parameters. The thickness of the cardboard was set to represent the three layers of the corrugated cardboard compressed together. This means that the air voids within the cardboard were ignored as diffusion through these spaces should be much faster than it would be through the cardboard.

The model was initialised to represent the set-up process used in the experiment, i.e. the flux out of the permeation accessory was allowed to equilibrate before it was placed in the chamber. The model was run for 1 h for the flux to equilibrate, then the vapour concentration within the chamber, but not within the permeation accessory, was set to zero.

The number of permeation layers, $n_{layer}$, for the PE film on the permeation accessory ($d_{total} = 130 \times 10^{-6}$ m) was set to 20, therefore $d_{layer} = 6.5 \times 10^{-6}$ m. The results converged with $d_{layer}$ for the cardboard and PTFE set to $2.5 \times 10^{-6}$ m and $5 \times 10^{-6}$ m respectively, ($n_{layer}$ was equal to 200 for both materials). This was because the material with the higher solid phase diffusion coefficient required a thinner $d_{layer}$. For the cardboard $d_{total} = 0.5 \times 10^{-3}$ m. For the PTFE, the actual wall thickness was $10 \times 10^{-3}$ m but $d_{total}$ was set to $1 \times 10^{-3}$ m, as in the model for the first validation experiment.

### 3.1.3. Permeation of vapour through a cardboard box into a room

For the third set of experiments, an EGDN vapour source was placed in a sealed cardboard box which was placed on a table in a room. The corrugated cardboard box was 20 cm × 20 cm × 20 cm (8 L) and all joints and edges were sealed using impermeable metal tape. Fig. 5 shows the set-up. A small amount of EGDN on an inert material (Kieselguhr) was placed within a permeation cell which was then covered in 130 µm thick PE film. Two of these permeation cells were placed within the cardboard box (see Fig. 6). The sides of the cardboard box had a single thickness of corrugated cardboard, whereas the top and bottom faces of the box were double thickness where the box flaps had been folded over. The table was covered in a sheet of tin-foil to reduce the sorption to the table.

The experiments were conducted in an air-conditioned room. Temperature and humidity loggers were placed upstream of leading corner of the box. The median temperature during the experiment was 24.5 °C with a standard deviation for each experiment of 0.6 °C. The median relative humidity was 49.5% with a standard deviation of 2.7%.

As in the second validation experiments, the PE covered permeation cells containing EGDN were allowed to equilibrate at 25 °C (the approximate temperature of the room) for 1 h before they were placed in the cardboard box.

Three experiments were run simultaneously side by side in the laboratory (see Fig. 5). In order to simplify the modelling, a AM08 Dyson Cool Pedestal Fan (Dyson, Wiltshire, UK) was used to blow air over the cardboard box at a reasonably steady rate. Without the fan, the air flow in the room would vary considerably during the experiment as people moved around the room to take measurements. The box was positioned with a corner edge facing the flow.

Measurements were taken of the air flow in the room. Velocity profiles were measured along vertical and horizontal lines at the fan and between the fan and the box. The measurements were

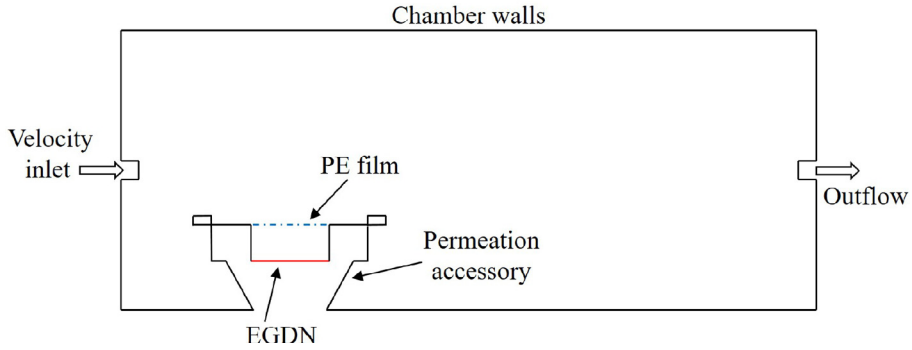


**Fig. 4.** Diagram showing the model geometry for the second validation experiment. Chamber dimension are given in Section 3.1.1.

**Fig. 5.** The cardboard box in lab experimental set-up, showing the triplicate experiments.

**Fig. 6.** The two permeation cells inside the cardboard box.

repeated for each box/fan set-up. The measurements were made using a TSI VelociCalc® model 9515 (Minnesota, USA).

The profiles measured at the fan were similar for all three set-ups, with maximum velocities of between approximately 2.0 m $s^{-1}$ and 4.0 m $s^{-1}$. The velocity in the centre of the fan was approximately 0.4 m $s^{-1}$.

The purpose of the third validation exercise was to test the vapour sorption/permeation part of the CFD model rather than the model's ability to predict the air flow in the room. Therefore, the data measured at the fan was used to define the boundary conditions while the data measured between the fan and the box was used to tune to model to achieve the correct air flow. Tuning was achieved by altering the turbulence intensity at the velocity inlet.

Vapour was sampled from around the outside of the box at various times during the experiment and then the air within the cardboard box was sampled at the end of the experiment.

**Table 3**
Vapour parameters for EGDN permeation used in the cardboard box in room model at 25 °C.

| | $C_0$/kg $m^{-3}$ | $D_m$/$m^2$ $s^{-1}$ | $D_{solid}$/$m^2$ $s^{-1}$ | $K_{ab}$ | $K_{ad}$/m |
|---|---|---|---|---|---|
| EGDN | $6.3 \times 10^{-4}$ | $8.8 \times 10^{-6}$ | | | |
| PE | | | $1.9 \times 10^{-12}$ | $2.2 \times 10^{3}$ | |
| Corrugated card | | | $5.7 \times 10^{-12}$ | $7.3 \times 10^{3}$ | |
| Permeation cell | | | | | 0.56 |
| Tin-foil | | | | | 1.26 |

The vapour concentrations outside of the boxes were measured at locations shown in Fig. 7. Samples at $X_2$ to $X_5$ were taken in the middle of the side of the box at 1 cm from the face. $X_1$ is located 0.5 m upwind from the middle of the front edge of the box and $X_6$ is located 0.5 m downwind from the middle of the back edge of the box. The air was sampled at 1 L $min^{-1}$ onto Tenax™ air sampling tubes for times varying from 1 min to 10 min depending on the expected concentration. At the end of the experiment (25 h) the air inside the box was sampled at 1 L $min^{-1}$ for 10 min by inserting a sample tube in through a hole cut in the top of the box.

The permeation properties for EGDN through PE and cardboard and the volatility and molecular diffusion coefficient for EGDN were calculated or measured using the same methods as described previously. It was assumed that $D_{solid}$ and $K_{ab}$ for cardboard were not a function of the thickness of the material. The partition coefficient for adsorption of EGDN vapour onto the tin-foil table covering, $K_{ad}$, was approximated using a model for SVOC adsorption onto stainless steel [25]. An adsorption coefficient for the permeation cell was calculated from previous experiments (not shown here). All these parameters are given in Table 3.

The set-up for the CFD model was as follows. The cardboard was modelled in the same way as it was in the second validation experiment model i.e. the thickness of the material was set to represent the three layers of the corrugated cardboard compressed together. The cardboard was $2.10 \times 10^{-3}$ m thick uncompressed and $3.15 \times 10^{-4}$ m thick compressed.

To simplify the CFD model, only a single box/fan set-up was modelled and the walls and ceiling of the room were not included. Symmetry was used to model only half of the single box/fan set-up. The fan was represented as a velocity inlet. A face on the opposite side of the domain to the fan was set as a outflow boundary. The side and top faces of the domain were set to symmetry boundary conditions. The floor, table and sides of the box were given no-slip boundary conditions. The $k-\omega$ SST turbulence model [23] was used along with the blended wall function options in the UDF, Eq. (8). Sorption through the PE film covering the permeation accessory and sorption onto the accessory used the laminar wall function option (Eq. (9)). A void below the box was included in

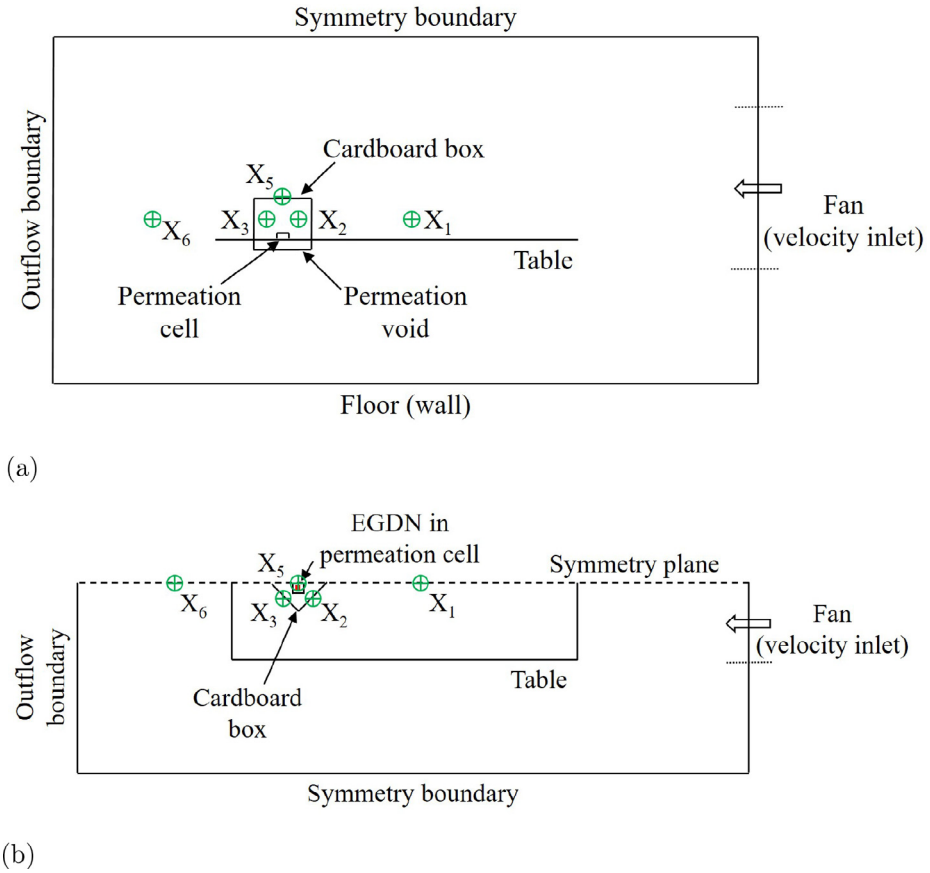


**Fig. 7.** Diagram showing the model geometry for the third validation experiment, showing side elevation (a) and plan view (b). The green crosses show the sample locations, the dotted lines are construction lines. (For interpretation of the references to colour in this figure, the reader is referred to the web version of this article.)

the model to allow vapour permeation into the cardboard at the bottom of the box. A diagram of the model is shown in Fig. 7.

A turbulent kinetic energy source term was added to the room to represent the mixing produced by the processes in the room which were not modelled explicitly. Primarily this was the air movement produced by two air conditioning units located on one of the walls. The source term was calculated using the assumption that all the kinetic energy (KE) produced by the air movement from the air conditioning units was converted to TKE and that it was distributed uniformly across the room. Eq. (10) gives KE per time or power [26].

$$\frac{\mathrm{KE}}{t} = \frac{1}{2} A \rho U^3, \tag{10}$$

where $t$ [s] is the time, $A$ [m$^2$] is the area of the air conditioning vent opening and $U$ [m s$^{-1}$] is the mean velocity at the opening. For this room the TKE source was 0.028 kg m$^{-1}$ s$^{-3}$.

As mentioned previously the velocity profile across the fan was based on the measured air flow. A high turbulence intensity at the inlet was required (40%) in order for the predicted velocities between the fan and the box to match those measured.

The velocity inlet at the fan was given a constant concentration boundary condition and was set to the concentration measured at $X_1$ at the 1 h sampling time. This was done to represent the background vapour concentration in the room.

The permeation accessory was meshed using the same approach as used in the second validation experiment model. The mesh on the outside of the cardboard box was kept sufficiently fine to achieve an area weighted average $y^+$ (a non-dimensional near-wall cell distance) of less than 5. A mesh dependency study was conducted on a similar model and this showed that the flow solution around the box was not significantly affected by a further mesh refinement. The effect of a further mesh refinement on the EGDN concentrations recorded at the sample locations was less than or equal to the difference due to the uncertainty in the sorption/permeation input parameters. The time step size was 0.2 s. It was shown that there was no significant change in the concentrations recorded at the sample locations with a smaller time step size.

The number of permeation layers, $n_{layer}$, for the PE film on the permeation cell was set to 20. The results converged with $d_{layer}$ for the cardboard set to $6.6 \times 10^{-6}$ m, i.e. $n_{layer} = 48$ for single thickness corrugated cardboard and 96 for double thickness corrugated cardboard.

### 3.2. Validation results

#### 3.2.1. Flow of vapour through a chamber with permeable walls

The vapour-air mixture flowed into the chamber through the narrow inlet with a velocity of 0.1 m s$^{-1}$. The velocity on the axis then decayed to less than 0.001 m s$^{-1}$ as the flow expanded to fill the chamber. At the end of the simulation, the there was only a small variation in vapour concentration across the PTFE chamber. The outlet concentration, $C_{out}$, from the chamber for the first validation experiment is shown in Fig. 8. The model performed well and is within the experimental data at most time points.

For future modelling, consideration should be given to the values of $d_{layer}$, $n_{layer}$ and $d_{total}$. Ideally $d_{total}$ should be set to the actual thickness of the material, but where this is not possible, a smaller value can be used as long as $t_{lag}$ remains long compared to the duration of the simulation. Model convergence was reached

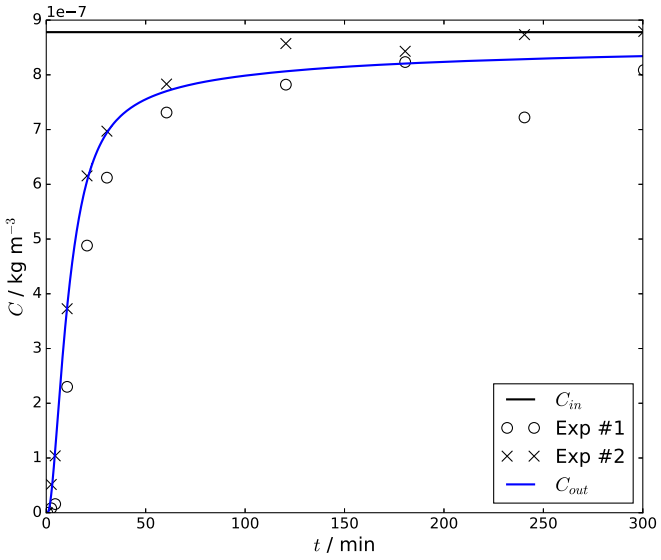


**Fig. 8.** Outlet concentration, $C_{out}$, from the PTFE chamber.

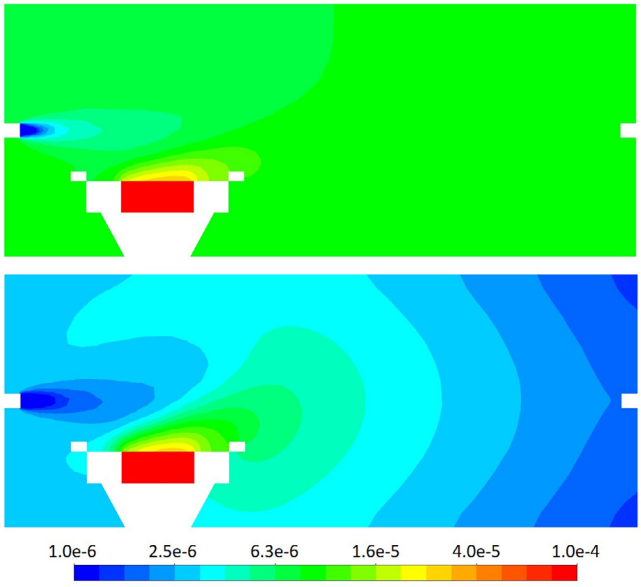


**Fig. 9.** EGDN concentration contours [kg kg$^{-1}$] on the symmetry plane at 360 min for the unlined chamber (upper) and carboard lined chamber (lower). Contours are shown with a log scale and are not clipped to the range.

in this case when $d_{layer}$ reached $1 \times 10^{-5}$ m. However, this value is likely to be dependent on $D_{solid}$, with thinner layers required for vapours with larger solid phase diffusion coefficients.

The results above have shown that the new permeation model can give accurate results for this type of scenario (laminar flow through a chamber with permeable walls) when suitable parameters are chosen.

### *3.2.2. Permeation of a vapour into and through a chamber with permeable walls*

EGDN concentration contours for the unlined and carboard lined chambers are shown in Fig. 9. These show how the vapour within the permeation cell permeated through the PE film and was then carried by the clean air entering the chamber along toward the outlet. The concentrations within the carboard lined chamber were lower that the unlined chamber and this was due to more absorption of the vapour into the cardboard than the PTFE alone.

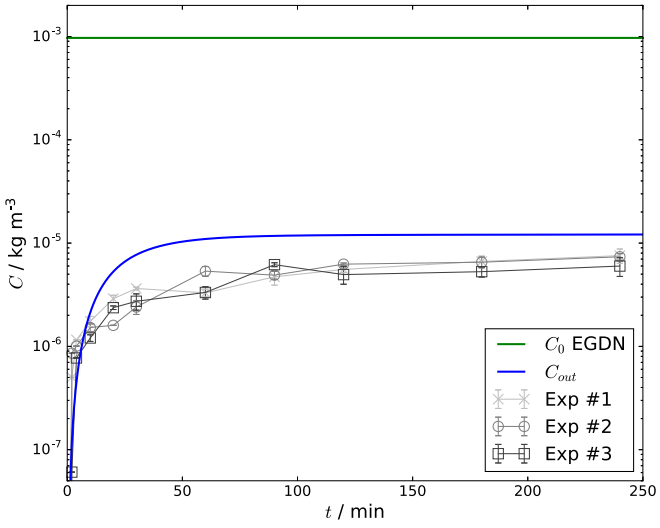


**Fig. 10.** Outlet concentration, $C_{out}$, from the unlined chamber. The error bars on the experimental data indicate one standard deviation from three replicate measurements. The green line shows the highest vapour concentration in the model i.e. the EGDN volatility. (For interpretation of the references to colour in this figure, the reader is referred to the web version of this article.)

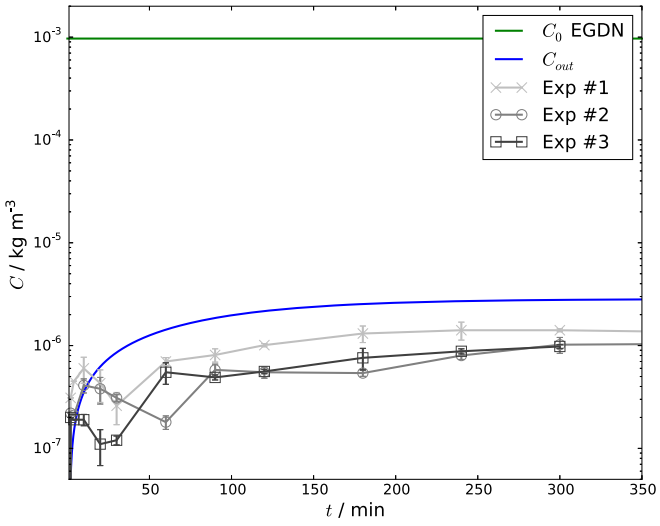


**Fig. 11.** Outlet concentration, $C_{out}$, from the cardboard lined chamber. The error bars on the experimental data indicate one standard deviation from three replicate measurements. The green line shows the EGDN volatility. Only data up to 350 min is shown. (For interpretation of the references to colour in this figure, the reader is referred to the web version of this article.)

After 360 min the vapour flux from the EGDN source was $3.33 \times 10^{-8}$ kg m$^{-2}$ s$^{-1}$ for both the unlined and carboard lined chambers. The flux was also $3.33 \times 10^{-8}$ kg m$^{-2}$.s$^{-1}$ for the PE film, showing that equilibrium had been reached for this part of the system. The flux into the PTFE or cardboard walls of the chamber were $9.65 \times 10^{-12}$ kg m$^{-2}$.s$^{-1}$ and $1.97 \times 10^{-10}$ kg m$^{-2}$ s$^{-1}$ respectively, confirming that the flux into the cardboard was much higher.

Concentrations are plotted as line graphs for the unlined PTFE chamber in Fig. 10 and the cardboard lined chamber in Fig. 11. The green line shows the EGDN volatility i.e. the vapour concentration within the permeation cell. The CFD performed well in following both the trend and the magnitude of the experimental data. At 240 min for the unlined chamber and 300 min for the lined chamber, the CFD is within a factor of 1.5 and 1.7, respectively, of the maximum experimental data point. It is not known what caused

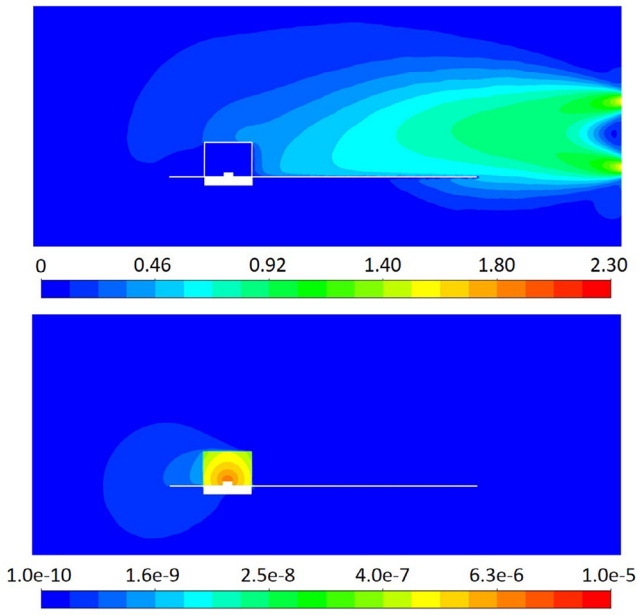


**Fig. 12.** Velocity contours [m $s^{-1}$] (upper) and EGDN concentration contours [kg $kg^{-1}$] (lower) at 24 h. Both sets of contours are shown on the (cropped) symmetry plane. The velocity contours are shown with a linear scale. The concentration contours are shown with a log scale and are not clipped to the range. The void below the box is included in the model to allow permeation into the cardboard at the bottom of the box.

the drop in the measured concentrations in the cardboard lined chamber at around 50 min (see Fig. 11) and this effect was not reproduced in the model.

The correlation between the model data and the experimental data is not as good as that shown in the first validation experiment. However, the set-up in this experiment was more complex, as it includes permeation of vapour into the chamber as opposed to the constant concentration in-flow in the experiment. There was also a very large range of concentrations in the domain in this experiment, from the saturation vapour pressure concentration inside the permeation cell to concentrations a couple of orders of magnitude lower than this at the outlet.

The quality of the CFD predictions support the assumption made when modelling the cardboard, i.e. that the diffusion through the air voids can be ignored.

It has been shown that this model is appropriate based on the correlation of the CFD data with the experimental data. However, it should be recognised that the CFD has consistently over-predicted the experimental data. It is not certain what caused this over-prediction, but it may be a result of some of the simplifying assumption used in the model. These include 1-dimensional permeation and an isotropic diffusion coefficient. There are also uncertainties in some of the input data, which may compound the effect. In spite of the over-prediction, the model can be used with confidence to predict the trends in the concentration profiles and the effect of using different absorbing materials for the walls of the chamber.

### 3.2.3. Permeation of vapour through a cardboard box into a room

Fig. 12 shows contour and velocity and concentration for the third validation model. The air flow generated by the fan can be seen moving towards and around the cardboard box on the table. The jets from the annular outlet of the fan converged within less than 0.5 m and the velocity of the air impacting on the box was approximately 0.4 m $s^{-1}$ or less. The concentration contours around the vapour source are symmetrical as transport within the box was driven by molecular diffusion only. After 24 h the vapour concentrations within the box were still much higher than those outside the box. As would be expected, there was very little vapour outside the front of the box and there was a plume of material in the wake of the box.

EGDN vapour concentrations at the monitor locations around the box are shown in Fig. 13. Both the experiment and the CFD give a lower concentration on the top of the box, $X_5$, compared to the back, $X_3$ and $X_4$. This is likely due to two factors. The concentrations on the inside of the top face of the box were lower compared to the back faces, as the top face was, on average, further from the source. Secondly, the air flow across the back was slower (as the flow separated from the corners of the box), so the permeating vapour was diluted less.

After 24 h the vapour flux from the EGDN source was $1.92 \times 10^{-8}$ kg $m^{-2}$ $s^{-1}$. This is less than the flux in the second validation model as this experiment was at a lower temperature. The flux through the single thickness sides of the box was approximately $1.30 \times 10^{-10}$ kg $m^{-2}$ $s^{-1}$ on average and from the double thickness top it was approximately $3.6 \times 10^{-11}$ kg $m^{-2}$ $s^{-1}$.

The model predictions are within or close to the experimental error bars at all time points for the locations close to the box ($X_2$, $X_3$ and $X_5$). Therefore, the model performs well in predicting the concentration around the box particularly considering the large range of concentrations present in the model (approximately eight orders of magnitude). The model does less well in predicting the concentration at $X_6$ at 24 h. However, as this is 0.5 m from the back edge of the box it is strongly influenced by the laboratory background concentration and therefore the inlet conditions set for the vapour concentration at the fan. All the other data shown in Fig. 13 was measured only 1 cm from the box.

The average of the vapour concentration measurements taken from within the box after 25 h was $4.8 \times 10^{-8}$ kg $m^{-3}$. This was significantly lower than that predicted by the model, $1.8 \times 10^{-6}$ kg $m^{-3}$. The main reason for the difference in these values is believed to be the inefficiency in the sampling method used in the experiment. It may also be that $D_{solid}$ and $K_{ab}$ for cardboard show some dependence on the thickness of the material.

A Tenax$^{TM}$ sample tube was inserted into the box and 10 L of gas was extracted. As the gas sample was drawn into the sample tube, fresh air would be drawn into the box and the most likely route for this air would be through the hole created for the insertion of this tube (the rest of the box was sealed using impermeable metal tape). Therefore, it is possible that there was a short circuit in the experiment with fresh air being sampled in preference to the air from the bottom of the box, where the concentration was higher. The measurement could be improved by taking a larger volume gas sample to increase the likelihood of removing all the vapour within the box and by inserting the Tenax$^{TM}$ tube further into the box.

Considering the complexity of the experimental set-up and the approximation of the flow around the box, it is felt that this model is appropriate to predict vapour concentrations around the outside of a cardboard box. The model should be used with caution when predicting in-box concentrations until the difference between the model and experimental data has been explained.

## 3.3. Validation discussion

The vapour sorption and permeation CFD modelling capability has been shown to perform well in a number of scenarios. However, the CFD model over-predicted the concentrations in the second validation experiment and significantly over-predicted the concentration of vapour present in the box at the end of the cardboard box experiment.

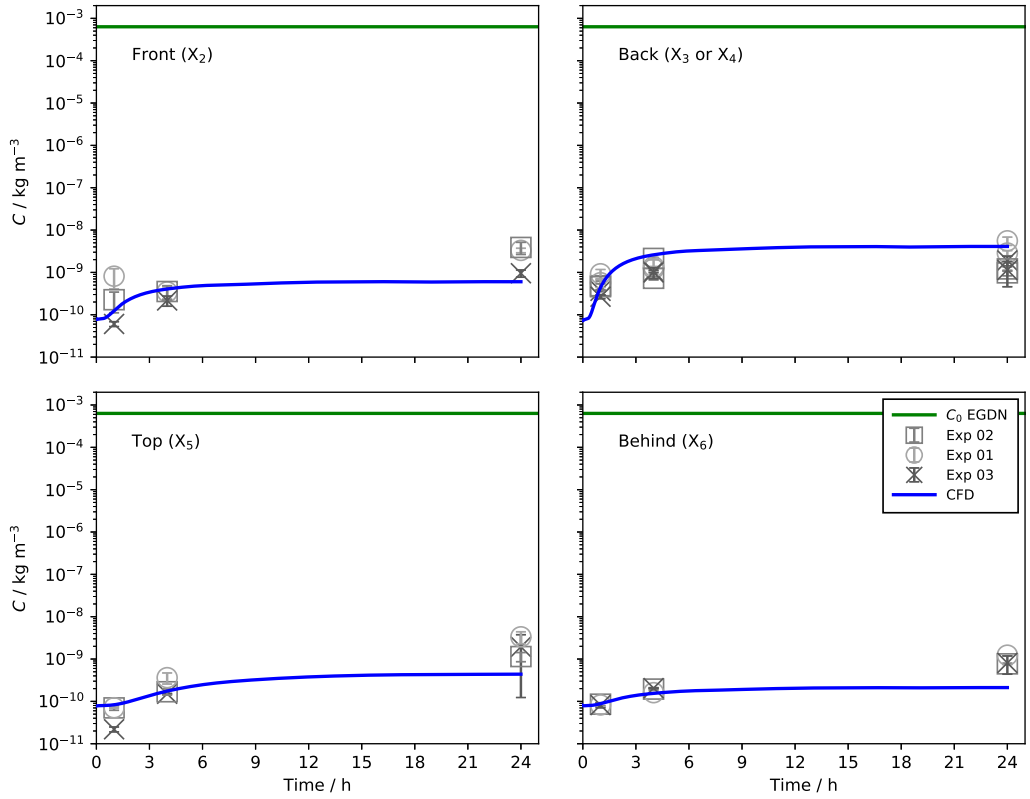


**Fig. 13.** Concentrations around the single unwrapped cardboard box. As only a symmetric half of the set-up was modelled, the data for $X_3$ is the same as for $X_4$. The error bars indicate one standard deviation from three replicate measurements. The green line shows the EGDN volatility. (For interpretation of the references to colour in this figure, the reader is referred to the web version of this article.)

Some of the model deficiencies could be due to uncertainties in the input data. A dependence of cardboard's permeation parameters on thickness being one of the possible causes. The model only represents 1-dimensional permeation, whereas permeation is likely to be more complex in some of the test cases examined. It was also assumed that the diffusion coefficient is isotropic, which may be true in PTFE and PE, but is unlikely to apply in corrugated cardboard. A possible explanation for the over-prediction of the vapour concentration within the box was the inefficiency in the vapour sampling method. It is recommended that the cause of the over-predictions be investigated further in the future.

The vapour permeation is sensitive to the thickness of the individual permeation layers, $d_{layer}$, and the sensitivity is strongest at the early stages of the simulation. It was shown that a thick permeable material can be represented in the model by a thinner material if the duration of the simulation is short compared to the lag time. This means that it is possible to specify thinner layers than would otherwise be possible (due to Fluent's limitation on the total number of UDMs).

The results for the simulations which included cardboard support the assumption that diffusion through the air voids in corrugated cardboard can be ignored. Therefore, the thickness of the cardboard in the UDF can be set to that of the three layers of the corrugated cardboard when compressed together.

Recognising the limitations described above, the vapour sorption modelling capability can now be used for scenario modelling when the setting consists of cardboard boxes or simple set-ups like the PTFE chamber experiment.

All the validation work reported here is for EGDN vapour only. Confidence in the capability would be improved if the validation could be extended to include a range of SVOCs and packaging materials.

## 4. Scenario modelling

The following scenarios, based around a cardboard box containing an explosive within a PE covered permeation cell, were modelled using the CFD modelling capability. These were selected to provide useful information to people conducting explosive vapour detection experiments on the relative importance of different factors which need to be considered.

1. How concentrations around a box containing EGDN varies with different types of cardboard. Two different types of cardboard, for which permeation data was available at the same temperature (30 °C), were considered. These were corrugated cardboard and single-ply cardboard.
2. How concentrations around a box containing EGDN vary at different temperatures, 25 °C and 35 °C.
3. How concentrations around a box containing either EGDN or trinitrotoluene (TNT) vary (at 35 °C).

These temperatures were chosen as it is simpler/quicker to conduct permeation experiments on low volatility material, such as TNT, at higher temperatures.

### 4.1. Scenario modelling set-up

All models were built and run using the set up described in Section 3.1.3. All models were solved for 24 h. All walls of the cardboard box were set to single thickness (corrugated or single-ply) cardboard only.

Permeation data, volatility and molecular diffusion coefficients were measured or calculated using the same methods as described before. This data is shown in Table 4. It should be noted that the corrugated cardboard tested at 30 °C was a different type

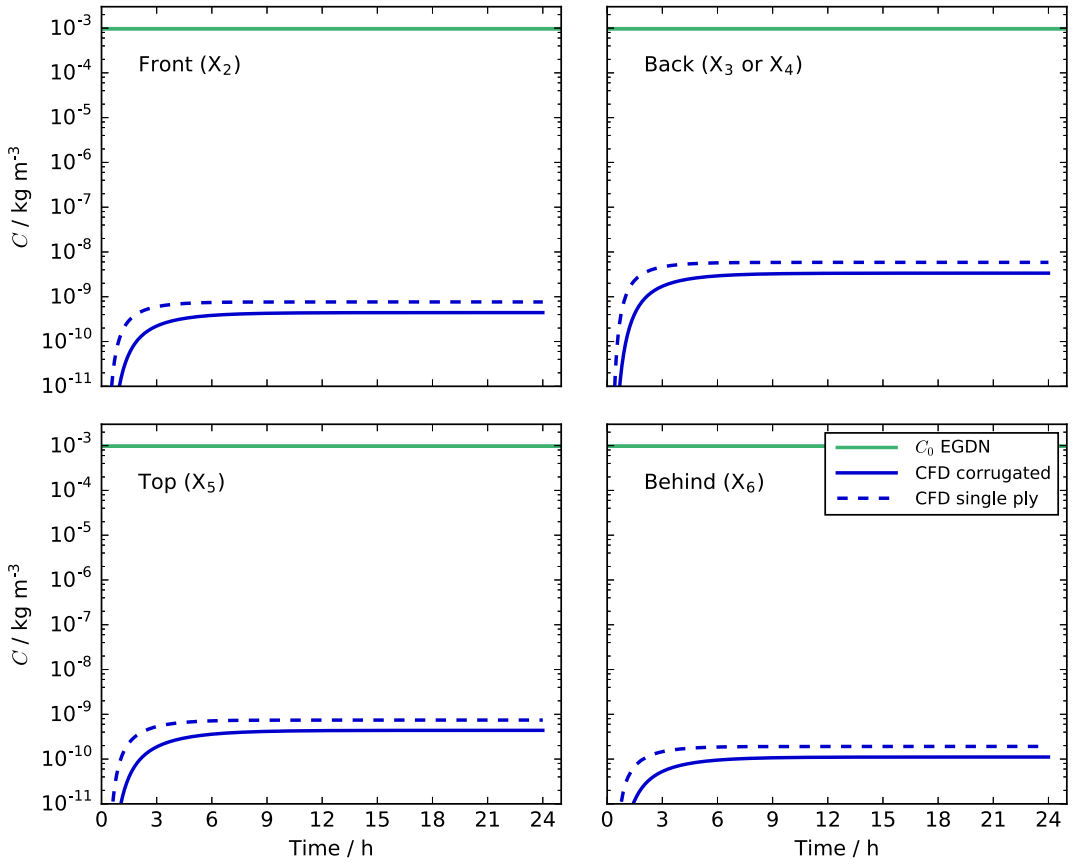


**Fig. 14.** Comparison between the vapour concentrations around a single cardboard box for two different types of cardboard at 30 °C.

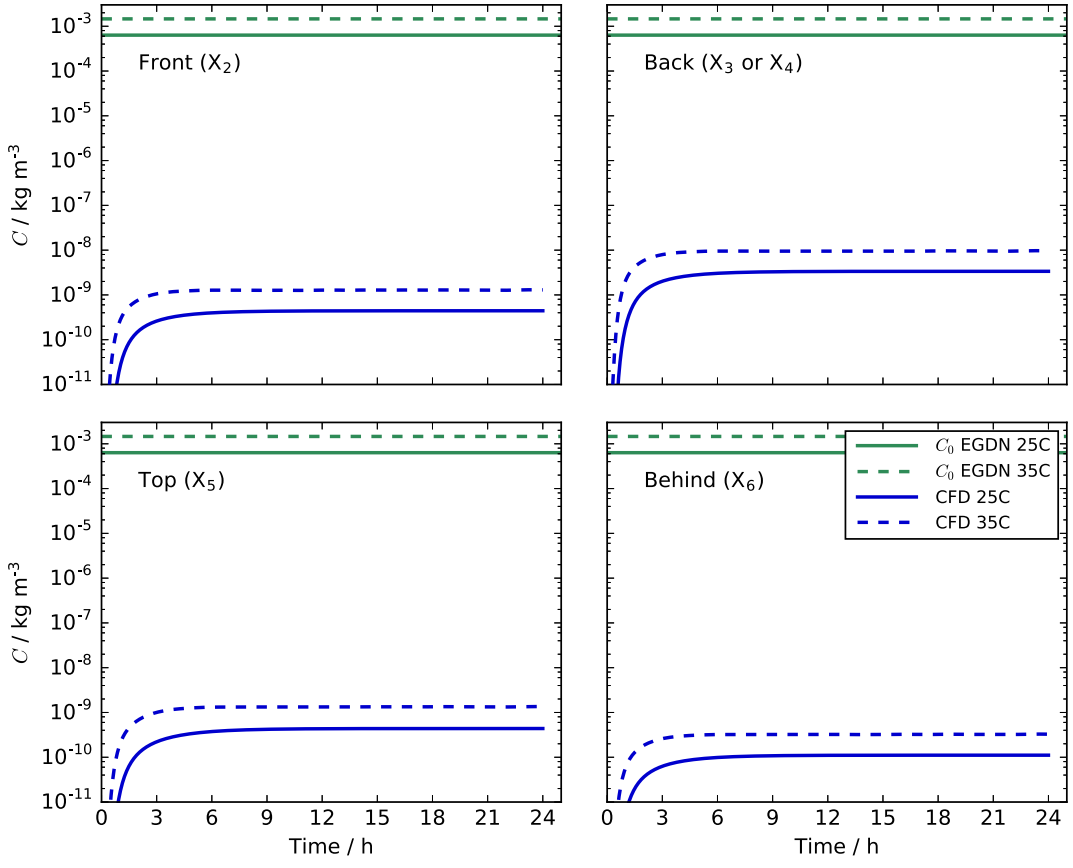


**Fig. 15.** Comparison between the vapour concentrations around a single cardboard box at two different temperatures.

**Table 4**
Vapour parameters used in the scenario modelling. The corrugated cardboard tested at 30 °C was a different type to that tested at 25 °C and 35 °C.

| Vapour | | $T$/°C | $C_0$/kg m$^{-3}$ | $D_m$/m$^2$ s$^{-1}$ | $D_{solid}$/m$^2$ s$^{-1}$ | $K_{ab}$ |
|---|---|---|---|---|---|---|
| EGDN | | 25 | $6.3 \times 10^{-4}$ | $8.8 \times 10^{-6}$ | | |
| EGDN | | 30 | $9.7 \times 10^{-4}$ | $9.0 \times 10^{-6}$ | | |
| EGDN | | 35 | $1.5 \times 10^{-3}$ | $9.3 \times 10^{-6}$ | | |
| | PE | 25 | | | $1.9 \times 10^{-12}$ | $2.2 \times 10^{3}$ |
| | PE | 30 | | | $2.5 \times 10^{-12}$ | $1.9 \times 10^{3}$ |
| | PE | 35 | | | $3.3 \times 10^{-12}$ | $1.6 \times 10^{3}$ |
| | Corrugated card | 25 | | | $5.7 \times 10^{-12}$ | $7.3 \times 10^{3}$ |
| | Corrugated card | 30 | | | $2.0 \times 10^{-11}$ | $1.7 \times 10^{3}$ |
| | Corrugated card | 35 | | | $9.1 \times 10^{-12}$ | $3.7 \times 10^{3}$ |
| | Single-ply card | 30 | | | $1.2 \times 10^{-10}$ | $1.5 \times 10^{3}$ |
| TNT | | 35 | $3.0 \times 10^{-7}$ | $7.1 \times 10^{-6}$ | | |
| | PE | 35 | | | $1.1 \times 10^{-13}$ | $7.1 \times 10^{5}$ |
| | Corrugated card | 35 | | | $2.8 \times 10^{-14}$ | $7.1 \times 10^{5}$ |

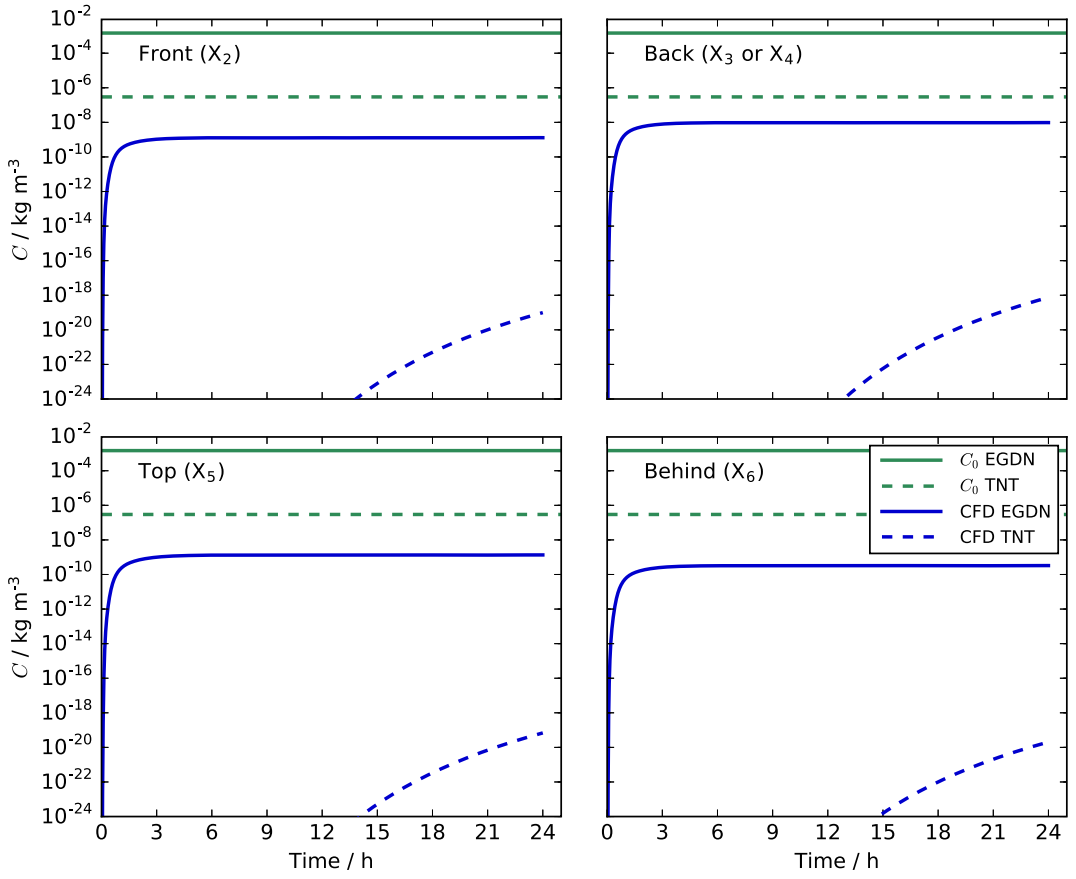


**Fig. 16.** Comparison between the vapour concentrations around a single cardboard box from EGDN and TNT 35 °C.

and thickness ($3.15 \times 10^{-4}$ m) to that tested at 25 °C and 35 °C, which was $5.00 \times 10^{-4}$ m thick. The single-ply cardboard was $1.15 \times 10^{-3}$ m thick.

### 4.2. Scenario results and discussion

#### 4.2.1. Scenario 1

Fig. 14 shows that changing the type of cardboard from single-ply cardboard to corrugated cardboard had only a small effect on the vapour concentrations predicted around the box. The concentrations after 24 h differ by a factor of approximatively 1.7. The flux through the cardboard is given by Eq. (11).

$$F = D_{solid}\, K_{ab} \frac{dC}{d_{total}}, \tag{11}$$

where $dC$ [kg m$^{-3}$] is the difference in concentration across the cardboard and $d_{total}$ [m] is the thickness of the cardboard. Therefore, for the same $dC$, the change in the equilibrium flux is equal to the change in $\frac{D_{solid} K_{ab}}{d}$. This value is only a factor of two (this factor is not to be confused with the factor of 1.7 difference in the concentrations given above) higher for the single-ply cardboard compared to the corrugated cardboard so explains the small difference in the equilibrium concentrations. The corrugated cardboard has a smaller $D_{solid}$ and is thicker, which will result in a longer lag time and the effect of this is the slightly slower rise in concentration.

#### 4.2.2. Scenario 2

Changing the temperature in the scenario changes the vapour pressure of the EGDN and the equilibrium flux changes by a similar amount, as shown in Fig. 15. As the temperature increases, $D_{solid}$

(in the cardboard and PE membrane on the permeation cell) increases but $K_{ab}$ (in the cardboard and PE membrane) decreases by a similar amount. This means that the change in flux is mainly due to the increase in EGDN volatility with temperature and the resulting increase in $dC$ across the walls of the box.

The EGDN vapour flux from the sides of the cardboard box after 24 h was $1.01 \times 10^{-10}$ kg m$^{-2}$ at 25 °C and $2.87 \times 10^{-10}$ kg m$^{-2}$ at 25 °C.

#### 4.2.3. Scenario 3

The difference between the concentrations of EGDN and TNT are significant as shown in Fig. 16. The diffusion coefficient for TNT through cardboard is more than two orders of magnitude less than that for EGDN; for diffusion through PE the difference is a factor of 30. The result of this is a significant increase in the lag time for TNT. The model has only been run for 24 h but it is expected that the equilibrium concentrations of TNT and EGDN will differ by a factor of approximately one tenth the difference in their vapour pressures. This is because $\frac{D_{solid} K_{ab}}{d}$ for cardboard is similar for both vapours but is an order of magnitude higher for TNT through PE.

The TNT flux through the cardboard after 24 h was far from equilibrium, with the flux into the cardboard still many orders of magnitude higher than the flux from the cardboard into the room. The EGDN flux was much closer to equilibrium. The TNT flux from the sides of the box was $1.74 \times 10^{-13}$ kg m$^{-2}$, the EGDN flux was $2.87 \times 10^{-10}$ kg m$^{-2}$.

## 5. Conclusions

A CFD based multi-layer sorption and permeation model has been developed and validated using three experiments of increasing complexity. The model uses a linear isotherm along with a blended wall function to represent near-wall transport. For input into the model, sorption/permeation data was generated for EGDN vapour transport through PE, PTFE and cardboard and TNT vapour through PE and cardboard.

Three scenarios where explosives were concealed within a cardboard box were modelled using the validated model. Some of the key variables: temperature, type of cardboard and type of vapour were varied to show how these changes affected the vapour concentration measured around the box.

The results of the scenario modelling showed that concentrations measured around the box were not strongly affected by the type of cardboard (corrugated to single-ply) or changing the temperature by 10 °C. Changing the explosive from EGDN to TNT had a significant effect and was more than can be explained by the change in vapour pressure alone. The large lag time for TNT vapour permeation through cardboard is a crucial factor affecting the concentration at early times.

The findings from the scenario modelling and the methods used to explain the differences in concentrations could be used when planning trials designed to assess the performance of detection equipment. They could also be used to help set requirements for detection equipment.

The CFD modelling approach developed can now be used to study a wide range of SVOC transport problems which would not previously have been possible.

## Declaration of Competing Interest

The authors declare that they have no known competing financial interests or personal relationships that could have appeared to influence the work reported in this paper.

## CRediT authorship contribution statement

**Timothy Foat:** Conceptualization, Formal analysis, Investigation, Methodology, Software, Validation, Visualization, Writing – original draft. **Joseph Drodge:** Formal analysis, Investigation, Software, Validation, Visualization. **Alexandra Charleson:** Formal analysis, Investigation, Methodology. **Barry Whatmore:** Conceptualization, Formal analysis, Investigation, Methodology. **Sophie Pownall:** Formal analysis, Investigation, Methodology. **Peter Glover:** Conceptualization, Methodology, Supervision. **James Nally:** Conceptualization, Software, Writing – review & editing. **Simon Parker:** Conceptualization, Writing – review & editing, Supervision. **Catherine Khan:** Conceptualization, Methodology, Supervision. **Andrew Marr:** Conceptualization, Methodology, Writing – review & editing, Supervision.

## Acknowledgements

The Fluent UDFs were written by Graham Macpherson, Dougal Ranford and Samuel Tabor of Frazer-Nash Consultancy Ltd. through a contract with Riskaware Ltd. We would like to acknowledge Megan Abbott, Monika Jurcic and Hannah McGinness for their work on the validation experiments and Steven Hawkins for his work on the UDFs. Timothy Foat would like to acknowledge the support of the Ph.D. scheme in the Faculty of Engineering and Physical Sciences at the University of Southampton.



## References

[1] C.J. Weschler, W.W. Nazaroff, Semivolatile organic compounds in indoor environments, Atmos. Environ. 42 (2008) 9018–9040.
[2] L. Wang, B. Zhao, C. Liu, H. Lin, X. Yang, Y. Zhang, Indoor SVOC pollution in china: a review, Chin. Sci. Bull. 55 (15) (2010) 1469–1478.
[3] R.G. Ewing, M.J. Waltman, D.A. Atkinson, J.W. Grate, P.J. Hotchkiss, The vapor pressures of explosives, TrAC Trends Anal. Chem. 42 (2013) 35–48.
[4] T.G. Foat, S.T. Parker, I.P. Castro, Z. T, Xie, Numerical investigation into the structure of scalar plumes in a simple room, J. Wind Eng. Ind. Aerodyn. 175 (2018) 252–263.
[5] T.A. Griffy, in: A Model of Explosive Vapor Concentration II, in Proceedings of the Fourth International Symposium on the Analysis and Detection of Explosives, Kluwer-Academic, New York, 1992.
[6] B. Singer, A.T. Hodges, H. Destaillats, T. Hotchi, K.L. Revzan, R. Sectro, Indoor sorption of surrogates for sarin and related nerve agents, Environ. Sci. Technol. 39 (9) (2005) 3203–3214.
[7] J.C. Little, C.J. Weschler, W.W. Nazaroff, Z. Liu, E.A. Cohen Hubal, Rapid methods to estimate potential exposure to semivolatile organic compounds in the indoor environment, Environ. Sci. Technol. 46 (20) (2012) 11171–11178.
[8] J. Xiong, C. Liu, Y. Zhang, A general analytical model for formaldehyde and VOC emission/sorption in single-layer building materials and its application in determining the characteristic parameters, Atmos. Environ. 47 (2012) 288–294.
[9] Z. Guo, A framework for modelling non-steady-state concentrations of semivolatile organic compounds indoors–I: emissions from diffusional sources and sorption by interior surfaces, Indoor Built Environ. 22 (4) (2013) 685–700.
[10] Y.-F. Mao, Z. Li, Y.-L. He, W.-Q. Tao, CFD analysis of SVOC mass transfer in different chambers, Int. J. Heat Mass Transf. 99 (2016) 613–621.
[11] P.A. Clausen, Z. Liu, Y. Xu, V. Kofoed-Sorensen, J.C. Little, Influence of air flow rate on emission of DEHP from vinyl flooring in the emission cell flec: measurements and CFD simulation, Atmos. Environ. 44 (23) (2010) 2760–2766.
[12] M.J. Lawson, B.A. Craven, E.G. Paterson, G.S. Settles, A computational study of odorant transport and deposition in the canine nasal cavity: implications for olfaction, Chem. Senses 37 (6) (2012) 553–566.
[13] X. Yang, Q. Chen, A coupled airflow and source/sink model for simulating indoor VOC exposures, Indoor Air 11 (4) (2001) 257–269.
[14] S. Murakami, S. Kato, K. Ito, Q. Zhu, Modeling and CFD prediction for diffusion and adsorption within room with various adsorption isotherms, Ultramicroscopy 97 (2003) 433–439.
[15] B. Deng, C.N. Kim, CFD simulation of VOCs concentrations in a resident building with new carpet under different ventilation strategies, Build. Environ. 42 (1) (2007) 297–303.
[16] Q. Zhang, G. Zhang, Study on TVOCs concentration distribution and evaluation of inhaled air quality under a re-circulated ventilation system, Build. Environ. 42 (3) (2007) 1110–1118.

[17] Y. Wang, B. Deng, C.N. Kim, Transient characteristics of VOCs removal by an air cleaner in association with a humidifier combined with different ventilation strategies in an office, Indoor Built Environ. 21 (1) (2012) 71–78.
[18] R.B. Jørgensen, T.H. Dokka, O. Bjørseth, Introduction of a sink-diffusion model to describe the interaction between volatile organic compounds (VOCs) and material surfaces, Indoor Air 10 (1) (2000) 27–38.
[19] Y. Zhang, J. Xiong, J. Mo, M. Gong, J. Cao, Understanding and controlling airborne organic compounds in the indoor environment: mass transfer analysis and applications, Indoor Air 26 (1) (2016) 39–60.
[20] J.P. Nally, S.T. Parker, C.J. Hindmarsh, Predictive modelling to assess low level hazards due to toxic chemical vapours, 2008, (Presented at the Chemical and Biological Defense Science and Technology Conference).
[21] B. Kader, Temperature and concentration profiles in fully turbulent boundary layers, Int. J. Heat Mass Transf. 24 (1981) 1541–1544.
[22] C.L.V. Jayatilleke, The Influence of Prandtl Number and Surface Roughness on the Resistance of the Laminar sub-Layer to Momentum and Heat Transfer, University of London, 1966 Ph.D. thesis.
[23] F.R. Mentor, Two-equation eddy-viscosity turbulence models for engineering applications, AIAA J. 32 (1994) 1598–1605.
[24] B.E. Poling, J.M. Prausnitz, J.P.O. Connell, The Properties of Gases and Liquids, fifth ed., McGraw Hill, Singapore, 2007.
[25] Y. Liang, Y. Xu, Improved method for measuring and characterizing phthalate emissions from building materials and its application to exposure assessment, Environ. Sci. Technol. 48 (8) (2014) 4475–4484.
[26] A. Kalmikov, K. Dykes, Wind power fundamentals, 2011, (http://web.mit.edu/windenergy/windweek/Presentations/Wind%20Energy%20101.pdf, Last accessed: 23-03-2021.